Proceedings of the 5th International Conference on Fluid Flow and Thermal Science (ICFFTS 2024)
Lisbon, Portugal- November 21 - 23, 2024
Paper No. 105
DOI: 10.11159/icffts24.105

Thermal Characterisation of a Wire Mesh Wick Vapor Chamber for Various Orientations

Wee Jian Ng[1,2], Vanessa Egan[1,2], Jeff Punch[1,2]
[1]CONNECT, Stokes Laboratories, Bernal Institute, University of Limerick, Ireland
[2]School of Engineering, University of Limerick, Ireland
Ng.weejian@ul.ie; Vanessa.egan@ul.ie; Jeff.punch@ul.ie

Abstract **-** In contemporary densified 5G base stations, different categories of electronic components (power devices, digital ICs) dissipate different levels of heat, causing challenges in terms of thermal segregation and temperature differences between nominally identical transmission channels. In such cases, a vapor chamber that acts as a passive two-phase heat transfer device could potentially become the solution by reducing both temperatures and temperature gradients across the base station. This study presents a method to accurately determine the thermal performance of a wire mesh-type vapor chamber (56 mm x 56 mm x 3 mm) with orientation angles ranging from 0° (horizontal) to 90°. In this method, an aluminium block is configured as a calorimeter that is in contact with the centre of the vapor chamber's evaporator, providing input powers ranging between 5 W to 60 W. One dimensional axial conduction is assumed to occur along the calorimeter, enabling the quantification of heat flow using local temperature measurements. The thermal performance of the vapor chamber is recorded in terms of thermal resistance, R_{th}, which is a standard metric to measure a material's ability to resist heat flow. For this experiment, R_{th} is measured between the evaporator and condenser, as a function of the range of input power levels, for different vapor chamber orientation angles: 0°, 30°, 45° and 90°. The results show that the vapor chamber is highly isothermal for all orientations. R_{th} of the vapor chamber at 0° is the lowest at ~0.5 K/W and reaches its highest at 90° with value of ~0.6 K/W at 60 W. These results set a foundation for the deployment of vapor chambers in densified 5G base stations, providing a solution for effective thermal extraction and isothermalisation of the structure.

Keywords**:** Vapor chamber, passive cooling, thermal characterisation, isothermalisation, thermal segregation.

1. Introduction

Mobile internet usage has increased to 4.6 billion people (57% of the global population), with 32% of this population covered by the fifth generation (5G) mobile network at the end of 2022 [1]. However, the range of a 5G cell signal is ~100 times less than a fourth generation (4G) cell, leading to a demanding >50 MC/km^2 (macro cells per kilometre squared) for 5G infrastructure in comparison to ~4-8 MC/km^2 for 4G. The upcoming sixth generation (6G) mobile network is expected to have an even lower cell range relative to 5G. Hence there is a clear need for more compact base stations for 5G and future networks [2, 3]. Typically, a base station features electronic devices that possess integrated circuits (ICs) with footprint areas of ~5-20 mm^2. In particular, power amplifiers, which dissipate the highest heat flux, are typically of area ~10 mm x 10 mm [4]. A challenge that arises with these base station configurations is an uneven distribution of heat flux, which results in thermal segregation from local "hot spots" [5]. The thermal challenge is further escalated when circuit boards are placed in a vertical orientation to meet form-factor and space-saving criteria of 5G base stations. As hot air rises, a bottom-to-top positive temperature gradient is introduced to the system, and devices located near the top of the base station are subjected to higher ambient temperatures.

To overcome this problem of non-isothermality, an integrated heat spreader (IHS) is commonly introduced to expand the effective surface area in between the electronic device and ambient. Although novel IHS materials are under development, copper (Cu) and aluminium (Al) are typically used as solid heat spreader materials due to their economical cost and high thermal conductivity, k. Prior work has shown that there is a threshold in the scale of heat spreaders above which solid materials such as Cu ($k \sim 10^2$ W/m.K) should be replaced with Vapor Chambers (VCs), planar two-phase heat transfer devices with very high effective thermal conductivity ($k_{eff} \sim 10^3$ W/m.K) [6-9]. For a heat source of area 10 mm x 10 mm, computational modelling [10] has shown that VCs progressively outperform Cu as spreader areas exceed 20 mm x 20 mm.

A VC is a two-phase heat transfer device that is typically square or rectangular in cross-section and consists of an internal chamber constructed with a porous medium (wick) along the internal top and bottom walls. The inner wick that is in contact with the heat source is called the evaporator, whereas the wall in contact with the adjacent heat sink is the condenser. At the evaporator, the working fluid evaporates and carries the heat away from the source surface. The vapor then condenses at the condenser, releasing latent heat that is dissipated out from the heat sink. The circulation is completed when the condensed liquid is recycled back to the evaporator through the porous wick via capillary force. Note that the two-phase flow circulation in VCs depends on the capillary pressure and permeability of the wick. Although there are multiple types of wicks – sintered powder wick, mesh wick, grooved wick, and composite wick – it is important to select a VC with a suitable wick for the required application. Most reported characterisations have been performed on either sintered copper powder wick VCs, or composite wick VCs that involve a wire mesh as part of their design. To the authors' knowledge, there are very few published studies on the most deployed coarse wire mesh wick VCs. In addition, for the characterisation process, it is not usual for the heat source to be at the size of power amplifier (~100 mm^2). Several studies on the characterisation of VCs applied heat sources with contact areas in the range of 225 to 900 mm^2, but only three previous studies used heat sources of ~100 mm^2 [11-13]. Of these three, only one employed a calorimeter approach, and this was on a sintered copper powder wick VC [13]. In this regard, there is a requirement to understand the thermal performance of wire mesh wick VCs with small-scale (~10 mm x 10 mm) heat sources. Moreover, in the context of base station applications, it is important to understand the influence of orientation. Several studies [11-16] have shown that a vertical (90°) placement resulted in a higher thermal resistance compared to the horizontal (0°) placement, however most of these studies focused on sintered copper powder wicked VCs. There was one study [17] that addressed mesh wicks, but this was a flat heat pipe, rather than a VC and results showed that the thermal resistance was highest when the heat pipe was oriented so that its evaporator was above the condenser.

In this paper, an off-the-shelf wire mesh wick VC is thermally characterised using a calorimeter, where the tip of the heat source is of dimensions 10 mm x 10 mm in order to represent the typical size of a power amplifier in a base station. Thermal characteristics are obtained for a range of tilt angles of the VC, from horizontal (0°) to vertical (90°), to quantify how performance may be affected in tilted base stations.

2. Experimental Method

This section introduces the experimental system (Fig. 1), the location of the surface temperature measurements on the wire mesh wick VC, and a frustum-tipped calorimeter. Twelve type-K thermocouples (RS PRO, 0.2 mm tip diameter) were embedded into the calorimeter (T_1 - T_3), as shown in Fig. 3(a), and attached to the surface of the VC (T_4 - T_{11} and T_0), as shown in Fig. 2(a) and (b). All temperature outputs were recorded by the Laboratory Virtual Instrument Engineering Workbench (LabVIEW) software, with measurement uncertainty of ±0.1 °C. A wire mesh wick VC (56 mm x 56 mm x 3 mm, T-Global Technology) with maximum operating power, Q_{max} of ~110 W, was tested in this experiment.

2.1. Experimental system

The experimental setup is as illustrated in Fig.1. The VC was initially tested in a horizontal orientation (0°) where the VC was perpendicular to gravity. Fig. 2(a) shows the heating surface located at the bottom centre of the VC and labelled as T_{tip}, with four thermocouples (T_4 - T_7) attached to the corners equidistant from the heat source. A set of thermocouple attachment pads (TAPS) were used to attach the thermocouples to the surface. Five thermocouples (T_0, T_8 - T_{11}), as shown in Fig.2(b), were attached to the top surface of the VC. To ensure good surface contact between the VC and the cooling block, narrow trenches were machined in the cooling block surface to allow a snug fit for thermocouple attachment. Between all surface contacts, a layer of non-silicone thermal grease (nominal thermal impedance of 0.012 °C-mm^2/W, RS PRO) was applied to ensure low contact resistance. All thermocouples were calibrated against a standard platinum resistance thermometer (SPRT) reference with ±0.1 °C uncertainty, and all temperature readings were recorded using the data acquisition software (LabVIEW).

Three ceramic cartridge heaters (ED3 24V) were installed at the bottom of the calorimeter, allowing a maximum thermal loading of 120 W. The testing power was limited by the operating temperature of the insulating block (RS PRO-PLA PRO+) and the thermal grease at 150 °C. To enhance the structural stability of the calorimeter and prevent direct contact between

the hot aluminium and the PLA enclosure, a 304 stainless steel plate was used as the base. Insulating wool was used to fill the empty space around the heating calorimeter to ensure minimal heat loss.

Heat removal was achieved through surface contact between the VC and the stainless-steel cooling block. The inlet temperature of the cooling block was set to a constant value of 10 °C. The insulating lid was printed with a space that could snugly fit the cooling block at the centre, helping to adjust the position between the attached VC and the calorimeter. A clamping mechanism was applied between the insulating lid and the stainless-steel base using screws at each corner, which were spring mounted to secure a consistent compression for surface contact between all the pieces, as shown in Fig. 2(c).

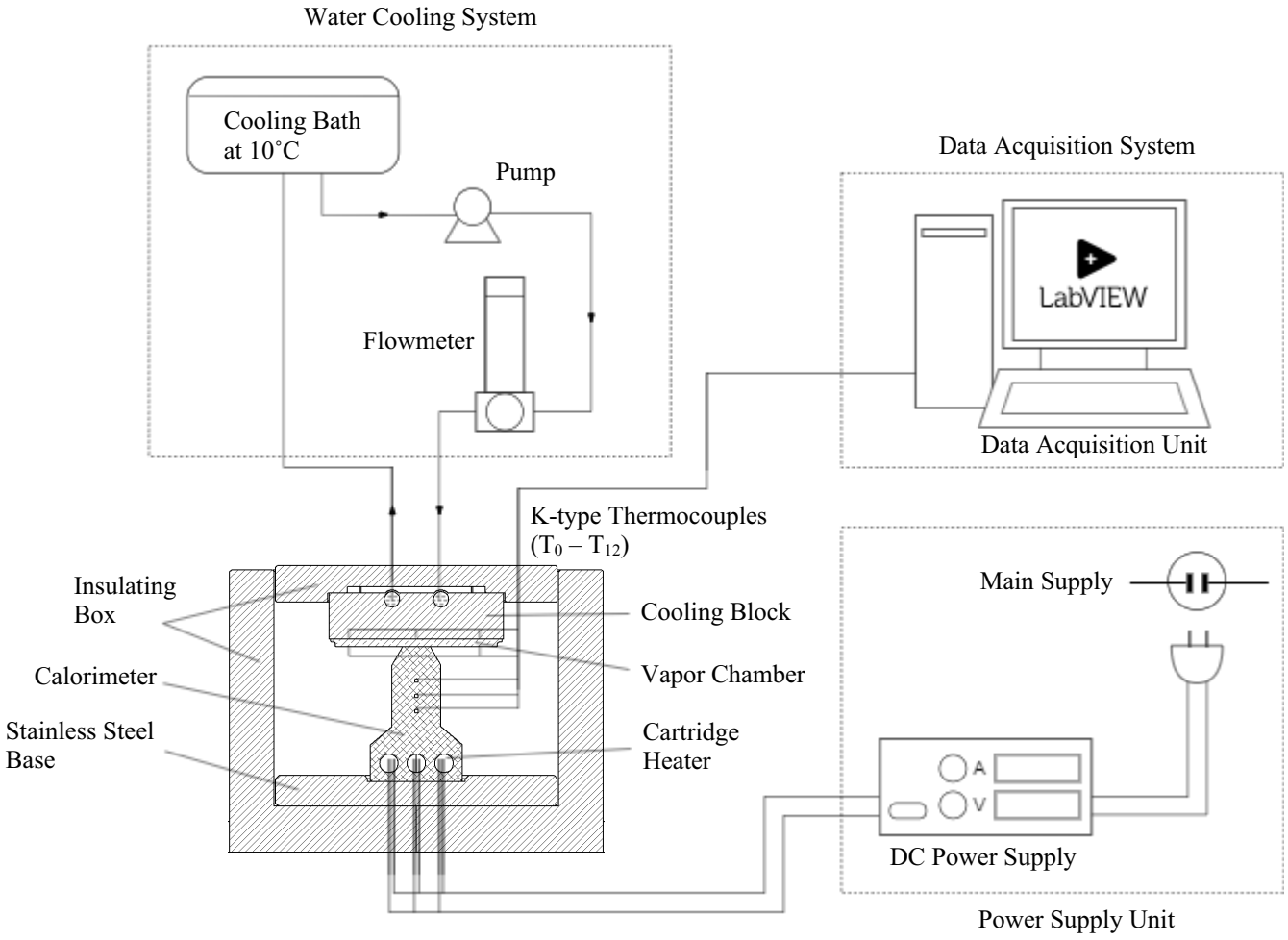

Fig. 1: Schematic of the experimental system with cross-sectional view of the clamping setup.

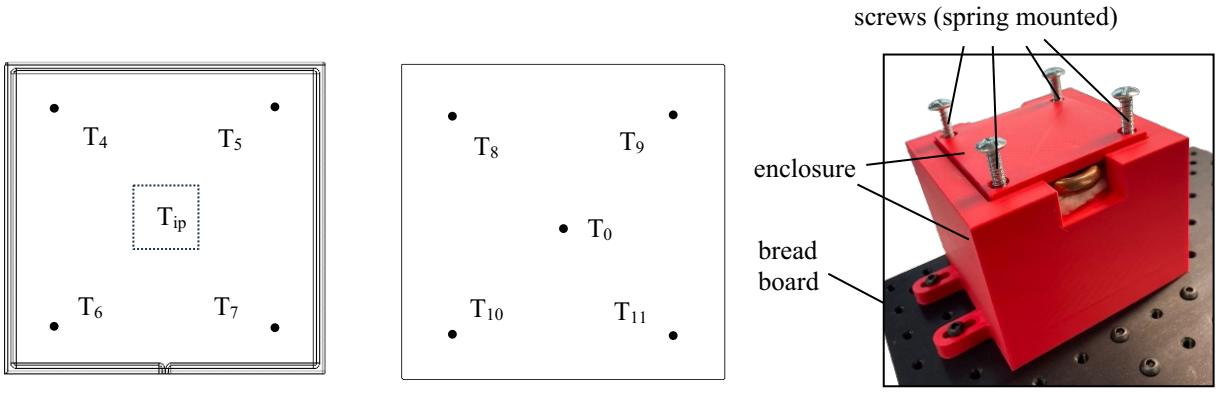

Fig. 2: Thermocouple distributions (a) on the bottom surface and (b) on the top surface, and (c) image of the enclosure showing the clamping setup.

2.2. Design of frustum tip calorimeter

The characterisation process was carried out using a calorimeter manufactured from aluminium (6082T6) to ensure light weight and high thermal conductivity (k = 180 W/m.K). The size of the tip was designed to be 10 mm x 10 mm in cross section to imitate the size of a power amplifier. The conventional ASTM D5470-06 standard [18] characterisation that uses a uniform cross section calorimeter was not suitable for this experiment, since a calorimeter with such a small cross section would make the experimental setup tall and complicated [16]. Fig. 3(a) shows the frustum-tipped calorimeter with square cross section throughout. The temperature T_e was extrapolated based on the ASTM D5470-06 standard, and the temperature, T_{tip} was calculated through integration based on equation 1 [19]:

$$q_x = -kA\frac{\mathrm{d}T}{dx} \tag{1}$$

$$k\left(T_e - T_{tip}\right) = q_x \tan^2\theta\left(\frac{1}{L\tan\theta - x} - \frac{1}{L\tan\theta}\right). \tag{2}$$

In the above expressions, q_x is the supplied thermal load, x is the ordinate in the direction of the heat transfer, L and θ is defined in Fig. 3(a). Initially, direct attachment of thermocouple to the frustum tip was considered to measure the temperature of the heat source. However, this approach would have affected the contact between the tip and the evaporator surface of the VC, hence the calculated value of T_{tip} was inferred as the evaporator temperature of the VC. The accuracy of the calculated value of T_{tip} was identified by comparing T_{tip} with the actual temperature at the tip measured using a thermocouple, labelled as T_m. The two sets of data were compared under thermal inputs of 2 – 15 W. Fig. 3(b) shows a line fitting plot based on the temperature difference, ΔT_{cal}, as shown in equation 3, and the maximum difference at 60 W will reach ~8.5 °C. It is suspected that the heat is lost to the surrounding because the calorimeter was not insulated when T_m was measured. Under such conditions, ΔT_{cal} is considered small and, hence, T_{tip} will be referred as the temperature at the evaporator of the VC throughout the experiment.

$$\Delta T_{cal} = T_{tip} - T_m \tag{3}$$

Note that as the calorimeter tip is small, this potentially affects the thermal contact resistance of the system which will be further discussed in section 3.1.

2.3. Data Reduction

The performance of a VC can be evaluated based on the total thermal resistance, which combines the conduction resistance and spreading resistance. Conduction resistance is defined as the one-dimensional resistance from the evaporator face to the condenser face, where the size of the heat source is the same size as the VC. Spreading resistance is the three-dimensional resistance from a concentrated heat source [19]. For this experiment, spreading resistance applies and is evaluated based on thermal resistance, R_{th}, which can be expressed as:

$$R_{th} = \frac{T_{tip} - \bar{T}_{top}}{Q} \tag{4}$$

where Q is the thermal load and $\bar{T}_{top}$ is the average temperature of the condenser surface of the VC, which can be defined as (refer to Fig. 3(b)):

$$\bar{T}_{top} = \frac{\sum_{i=8}^{11} T_i + T_0}{5}. \tag{5}$$

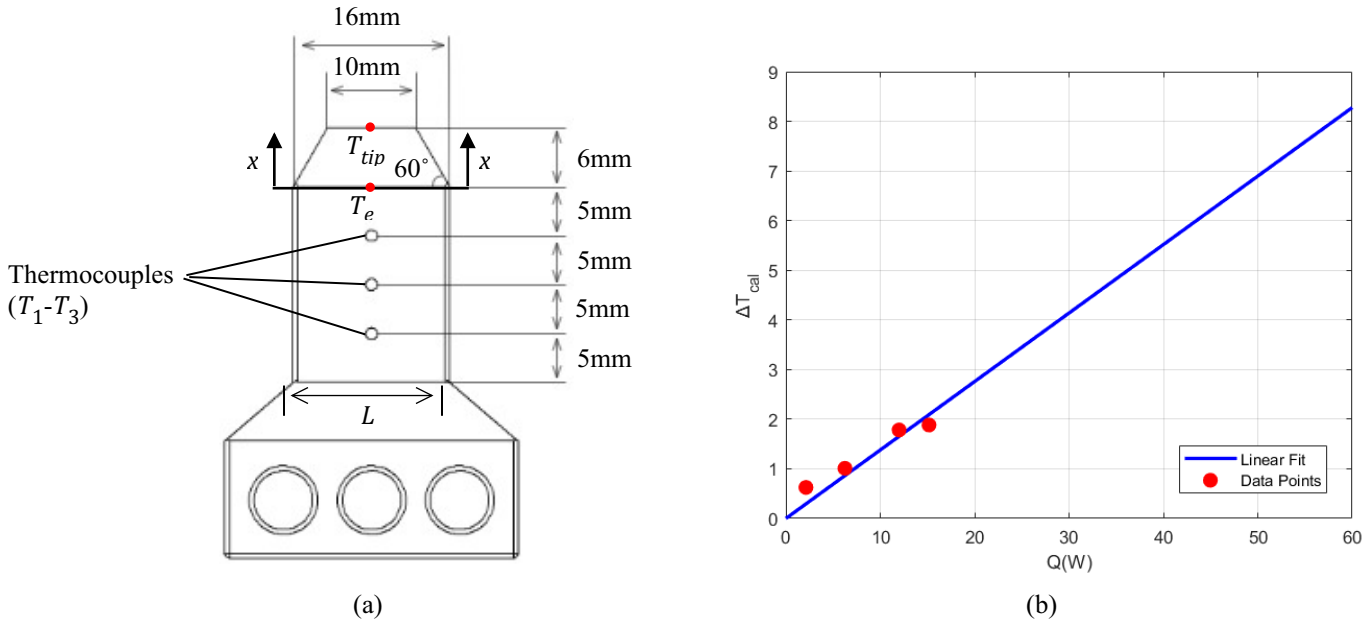

Fig. 3: (a) Schematic of the frustum-tipped calorimeter and (b) temperature difference between T_m and T_{tip}.

Contact resistance has been a common factor that influences the characterisation of the uniformity of the temperature distribution of a VC, especially when the calorimeter tip is small relative to the VC evaporator surface, as shown in Fig. 2(a) and Fig. 3(a). To confirm the isothermality of the VC, the uniformity of the temperature distribution between the evaporator and the condenser surface of the VC is expressed as:

$$\Delta T = \bar{T}_{bot} - \overline{T_{top}} \tag{6}$$

where $\bar{T}_{bot}$ is the average temperature of the evaporator surface of the VC, which can be defined as (refer to Fig. 3(a)):

$$\bar{T}_{bot} = \frac{\sum_{i=4}^{7} T_i}{4}. \quad (7)$$

Note that the value of T_{tip} is excluded from $\bar{T}_{bot}$ to exclude the influence of contact resistance from the calorimeter.

3. Results and Discussion

This section details the characterisation of the wire mesh wick VC for a range of thermal loads and orientations. R_{th} and ΔT are discussed to show the effect of gravity and thermal contact resistance on the isothermality of VC. The temperature distribution at the condenser surface is analysed to determine the cause of the non-uniformity.

3.1. Thermal resistance behaviour of VC

Fig. 4(a) shows the thermal resistance of the VC for a range of orientations from 0° to 90°. The reference orientation of 0° shows an overall lower R_{th} that reaches a value of ~0.5 K/W at the maximum power level. This trend is similar to what is reported in the literature, where R_{th} reduces with increasing Q. The value of ~0.5 K/W falls within the range of values reported in the literature, ~0.04 – 0.85 K/W [6-19]. The R_{th} of the VC increases with tilt angle, with a vertical (90°) orientation having the highest R_{th} due to the capillary movement of the fluid working against gravity. Note that the VC's resistance at 30°, 45° and 90° converge gradually as the thermal load increases, showing that orientation has a larger impact on thermal performance at lower heat loads. Above 35 W, the thermal resistance difference between the horizontal VC and the other orientations is ~0.23 K/W, which is relatively small – an advantage in the context of tilted 5G base station applications.

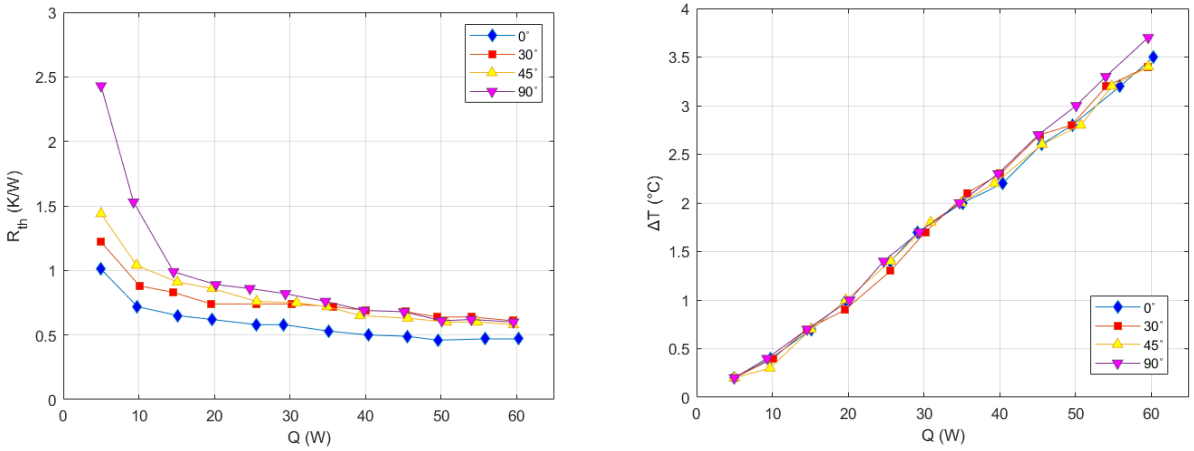

(a) (b)

Fig. 4: (a) Thermal resistance of VC and (b) average temperature difference between the evaporator and condenser surfaces of the VC as a function of input power under different orientations.

3.2. Isothermal properties of VC

In order to evaluate the isothermality of the VC, the influence of the heat source, T_{tip}, is excluded and the temperature difference, ΔT (equation 2) between the evaporator and condenser surfaces is plotted against the power input (Fig. 4(b)). As the heat load increases, the difference in ΔT at 60 W between VC orientations of 0° to 45° is 0.1 °C, whereas the difference between 0° to 90° is 0.2 °C. The ΔT plot presents minimal difference between each orientation, showing that the VC, as a heat transfer device itself, is highly isothermal. If Fig. 4(a) and (b) are compared, the R_{th} plot reveals differences at every

orientation, showing that T_{tip} is a very significant factor in illustrating the heat transfer characteristic of the VC. Although gravity influences the capillary movement of the fluid within the wick, it is also suspected that the thermal contact resistance between the calorimeter and the VC may vary with orientation angle. All parts in the test rig are clamped together in a top-down direction hence, when the rig was tilted, especially to 90°, the clamping force may have featured an offset, which would affect the thermal contact resistance – an effect which would be exacerbated because of the size of the calorimeter tip (10 mm x 10 mm). Nevertheless, thermal contact resistance is a prevalent challenge for small- and medium-sized ICs, which would also afflict VCs in practical base station applications.

Fig. 5 presents the temperature distribution of the bottom and top surfaces of the VC under different orientations at Q = 60 W. At the 90° orientation, both plots show higher temperatures at all data points, demonstrating the effect of gravity. Fig. 5(a) highlights the significantly lower temperature of the T_{tip} at 0°, showing that the VC does perform notably better in a horizontal orientation. If T_{tip} is excluded, a comparison of Fig. 5(a) and (b) shows that the highest temperature difference between the evaporator and the condenser surfaces is less than 8 °C (between T_4 and T_8) at 90°. Fig. 5(b) shows a temperature difference of no more than 5 °C (between T_8 and T_{11}) in general. These show that the VC exhibits a very high effective thermal conductivity that strongly promotes isothermality. Fig. 5(b) shows a non-uniformity that is mainly caused by the water-cooling system. T_8 and T_{11} are located near the inlet and outlet ports of the water-cooled block, respectively, which induces differences related to a temperature gradient in the direction of flow.

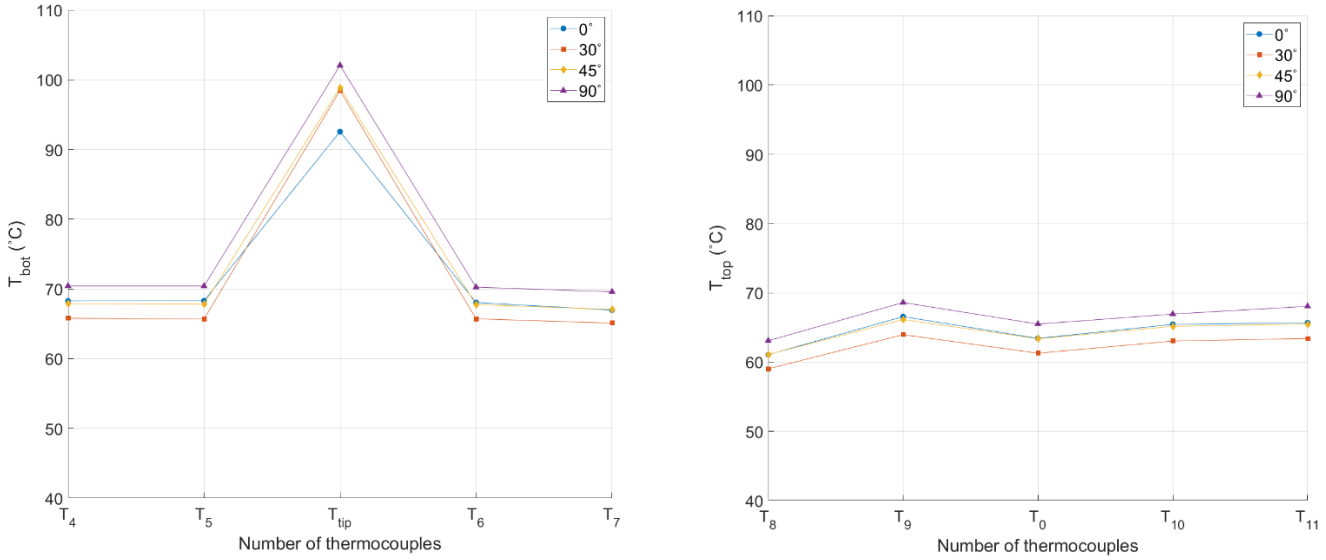

Fig. 5: Temperature distribution of the (a) evaporator surface and (b) condenser surface of the VC at Q = 60 W.

4. Conclusion

The thermal performance of a wire mesh wick VC was studied under varying orientations (0°, 30°, 45° and 90°). By taking 0° as reference, the R_{th} and ΔT between evaporator and condenser surfaces, and the spatial temperature distributions, were analysed. The conclusions are as follows:

1) Across all sets of parameters (input power and orientations), the wire mesh VC shows low thermal resistance (~0.5-2.5 K/W). At input powers of > 20 W, the thermal resistance drops below 1 K/W, demonstrating a competitive thermal resistance compared with other heat transfer devices.
2) For all different orientations, R_{th} decreases by ~50 – 75% across increasing power inputs of 5 – 60 W.

3) Thermal resistance increases with increasing tilting angle and peaks at a vertical (90°) orientation. However, the average temperature difference between the evaporator and condenser suggests that the VC is highly isothermal regardless of the orientation of the VC. This result shows that VCs can provide a solution to the formation of 'hotspots', and can be practically applied in vertically oriented 5G base stations.
4) The VC performance is at its best at power inputs > 35 W, making it a suitable heat spreader for ICs in 5G base stations, especially for power amplifiers that dissipate high thermal loads.

Acknowledgements

This research is conducted with the financial support of Science Foundation Ireland (SFI) under Grant Number. 13/RC/2077_P2.

References

[1] GSMA (2023). The State of Mobile Internet Connectivity 2023 [Online]. Available: https://www.gsma.com/r/wp-content/uploads/2023/10/The-State-of-Mobile-Internet-Connectivity-Report-2023.pdf
[2] X. Ge, S. Tu, G. Mao, C. X. Wang and T. Han, "5G Ultra-Dense Cellular Networks," *IEEE Wireless Communications*, vol. 23, no. 1, pp. 72-79, February 2016.
[3] M., Dileep & Jena, Mr. Soumya*, "*Challenges and Future Research Directions in 6G*" in 6G Technology and It's Applications,* Dwalior, MP: Xoffencer, 2023, pp. 119-136.
[4] T. Cappello, P. H. Pednekar, C. F. Steve, C. Cripps, Z. P. Taylor and W. Barton, "Supply and Load Modulated Balanced Amplifier for Efficient Broadband 5G Base Stations," *IEEE Transactions on Microwave Theory and Techniques,* vol. 67, no. 7, pp. 3122-3133, July 2019.
[5] R. Prasher and J.Y. Chang, "Cooling of electronic chips using microchannel and micro-pin fin heat exchangers," in *ASME 2008 6th International Conference on Nanochannels, Microchannels, and Minichannels*, Darmstadt, Germany, 2008, pp. 1881–1887.
[6] N. Lakhkar, A. Banerjee, G. Refai-Ahmed, and D. Agonafer, "Multiobjective optimization of graphite heat spreader for portable systems applications," in *Proceedings of the ASME 2009 InterPACK Conference*, San Francisco, California, 2009, pp. 571–578.
[7] D. Sabatino and K. Yoder, "Pyrolytic graphite heat sinks: A study of circuit board applications," *IEEE Trans. Compon., Packag., Manuf. Technol.*, vol. 4, no. 6, pp. 999–1009, June 2014.
[8] J. Zhang, G. Shi, C. Jiang, S. Ju, and D. Jiang, "3D bridged carbon nanoring/graphene hybrid paper as a high-performance lateral heat spreader," *Small*, vol. 46, pp. 6197–6204, 2015.
[9] Y. Zhang, H. Han, N. Wang, P. Zhang, Y. Fu, M. Murugesan, M. Edwards, K. Jeppson, S. Volz and J. Liu, "Improved heat spreading performance of functionalized graphene in microelectronic device application," *Advanced Functional Materials*, vol. 25, no. 28, pp. 4430–4435, 2015.
[10] J. Due and A. J. Robinson, "Reliability of thermal interface materials: A review," in *Applied Thermal Engineering*, vol. 50, no. 1, pp. 455–463, 2013.
[11] Y. Tang, D. Yuan, L. Lu and Z.Wang, "A multi-artery vapor chamber and its performance," *Applied Thermal Engineering*, vol. 60, no. 1-2, pp. 15-23, 2013.
[12] M. Tsai, S. Kang, K. V. Paiva, "Experimental studies of thermal resistance in a vapor chamber heat spreader," *Applied Thermal Engineering*, vol. 56, pp. 38-44, 2013.
[13] X. Ji, J. Xu, A. M. Abanda, "Copper foam based vapor chamber for high heat flux dissipation," *Experimental Thermal and Fluid Science*, vol. 40, pp. 93-102, 2012.
[14] Y. Xia, F. Yao, F and M. Wang, "Experimental Investigation on Thermal Performance of Vapor Chambers with Diffident Wick Structures," *Energies*, vol. 16, no. 6464, 2019.
[15] Z. Chen, Y. Li, J. Yu, L. Deng, H. Chen and X. Tang, "Fabrication and characterization of ultra-thin vapour chambers with printed copper powder wick," *Applied Thermal Engineering*, vol. 201, 2022.
[16] J. Ma, X. Luo and R. Hu, "Effect of inclination angle on the performance of a kind of vapor chamber," *Journal of Solid State Lighting*, vol. 1, 2014.

[17] G. Huang, W. Liu, Y. Luo, Y. Li, H. Chen, “Fabrication and thermal performance of mesh-type ultra-thin vapor chambers,” *Applied Thermal Engineering*, vol. 162, 2019.
[18] R. Kempers, P. Kolodner, A. Lyons and A. J. Robinson, “A high-precision apparatus for the characterization of thermal interface materials,” *Review of Scientific Instruments,* vol. 80, no. 9, 2009.
[19] A. J. Robinson, J. Colenbrander, R. Kempers and R. Chen, “Solid and Vapor Chamber Integrated Heat Spreaders: Which to Choose and Why,” *IEEE Transactions on Components, Packaging and Manufacturing Technology,* vol. 8, 2018.